VIP Heterogeneous Catalysis Very Important Paper

Zitierweise:
Internationale Ausgabe: doi.org/10.1002/anie.202208237
Deutsche Ausgabe: doi.org/10.1002/ange.202208237

Hydrogen Spillover and Its Relation to Hydrogenation: Observations on Structurally Defined Single-Atom Sites**

*Max J. Hülsey[+], Victor Fung[+], Xudong Hou, Jishan Wu, and Ning Yan**

Abstract: Hydrogen spillover, involving the transfer of H atoms from metal sites onto the catalyst support, is ubiquitous in chemical processes such as catalytic hydrogenation and hydrogen storage. Atomic level information concerning the kinetics of this process, the structural evolution of catalysts during hydrogen spillover, as well as the nature of participation of the spilled over H in catalysis, remain vastly lacking. Here, we provide insights to those questions with a solubilized polyoxometalate-supported single-atom catalyst which allows for the use of characterization techniques generally inaccessible to the study of heterogeneous catalysts. Hydrogenation kinetics together with poisoning studies further reveal that hydrogen spillover can be either detrimental or beneficial for catalysis, the direction and magnitude of which depends mostly on the nature of the reducible functional group. Similar trends were observed on one of the most prototypical hydrogen spillover catalysts—Pt/WO_3.

Introduction

Previously studied catalysts exhibiting hydrogen spillover only offer limited insights due to their lack of well-defined structures, insufficient tools to precisely characterize spillover stoichiometries and kinetics, as well as the lack of information on the role of spilled over hydrogen during catalysis.[1] For example, conventional nanoparticle catalysts on metal oxides such as the prototypical Pt/WO_3 comprise ill-defined metallic hydrogen splitting sites as well as complex metal support interfaces. Furthermore, ambiguities exist about whether spilled over H should be rather regarded as hydrogen atoms or protons.[2] Although surface science studies offer deeper insights, correlating hydrogen spillover with catalytic activity remains difficult.[3] In most cases, the support covered in spilled over hydrogen is viewed as a H reservoir with the metallic site as the main driver for catalysis, though in certain cases the direct participation of the H-covered support in hydrogenation reactions has been hypothesized.[1,4] Besides constraints by the catalyst materials, techniques to study the hydrogen spillover phenomenon are additionally restricted to solid-state NMR,[5] temperature-programmed reactivity studies,[6] neutron scattering,[7] resonant photoemission[8] and X-ray absorption spectroscopy,[9] among others, all with known limitations in the investigation of heterogeneous catalysts. DFT calculations can offer additional details but the relevance of those results is compromised by the lack of definedness of most heterogeneous catalysts exhibiting spillover.

Due to these limitations, several major questions about hydrogen spillover remain inconclusively addressed: i) the kinetics of the process, i.e. how the rate of H spillover is affected by an intermediate spillover state, ii) the composition and properties of the catalyst after H spillover, and iii) how the spilled over H contributes to heterogeneous hydrogenation catalysis. Herein, we provide insights to those questions by characterizing the hydrogen spillover behavior of several solubilized lacunary polyoxometalate (POM)-based single-atom catalysts (SACs). Previously, we reported similar catalysts to identify active sites during hydrogenation, as well as the CO and benzyl alcohol oxidation reactions.[10] The chemical space for POM-based (single-atom) catalysts has been drastically extended especially in the past few years opening exciting avenues for both discovering new catalytic reactivity as well as fundamental studies.[11] Herein, we find a unique interplay between positively charged Pd and a reducible Mo-based support for hydrogen spillover. Due to the solubility of the SAC in polar solvents, techniques like electrospray ionization mass spectrometry (ESI-MS), liquid phase ^{1}H NMR and UV/Vis spectroscopy become viable tools for the characterization of the process. Based on reaction kinetics, catalyst poisoning, and ESI-MS, we identified subtleties in the contribution of spilled over H to the hydrogenation of different substrates. These molecularly defined catalyst model structures with experimentally proven reaction intermediates provide an ideal system for DFT calculations to understand both the thermodynamics as well as kinetics of hydrogen spillover. Combined with analogous experiments with Pt/WO_3, it

[*] Dr. M. J. Hülsey,[+] Dr. N. Yan
Department of Chemical and Biomolecular Engineering, National University of Singapore
1 Engineering Drive 3, 117580 Singapore (Singapore)
E-mail: ning.yan@nus.edu.sg
Dr. V. Fung[+]
Center for Nanophase Materials Sciences, Oak Ridge National Laboratory
One Bethel Valley Road, Oak Ridge, TN 37831 (USA)
X. Hou, Dr. J. Wu
Department of Chemistry, National University of Singapore
3 Science Drive 3, 117543 Singapore (Singapore)
[+] These authors contributed equally to this work.

[**] A previous version of this manuscript has been deposited on a preprint server (ttps://doi.org/10.21203/rs.3.rs-574294/v1).

appears that our findings are not only true for SACs but may be more generally applicable.

Results and Discussion

SACs based on lacunary POMs offer advantages such as easy synthesis, stable structures in 1:1 metal support ratios, as well as their high solubility in polar solvents.[10d] $PMo_{11}O_{39}$ (charge states are omitted for clarity) was synthesized by the lithium carbonate-mediated removal of one MoO subunit from phosphomolybdic acid (Figure 1a, Figure S1) while $PW_{11}O_{39}$ was synthesized following a procedure described in our previous study.[10d] Mixing equimolar ratios of the lacunary POM and metal salts with weakly coordinating ligands yielded the active site in situ, $PMo_{11}O_{39}Pd_1$, which can be easily and unambiguously characterized by electrospray ionization mass spectrometry (ESI-MS) ($\{[PMo_{11}O_{39}Pd_1]+2H^+\}^{3-}$ (calc.: 606.55, expt.: 606.57; the formula in the brackets indicates the composition of the catalytic sites whereas the two protons are captured from the solvent). DFT calculations confirmed that Pd was most likely adsorbed in the vacant site of the lacunary POM similar to structures that were confirmed experimentally before (Figure S2).[12] We also precipitated $PMo_{11}O_{39}M_1$ (M = Pd, Pt, Rh) as tetrabutylammonium salts for solid-state

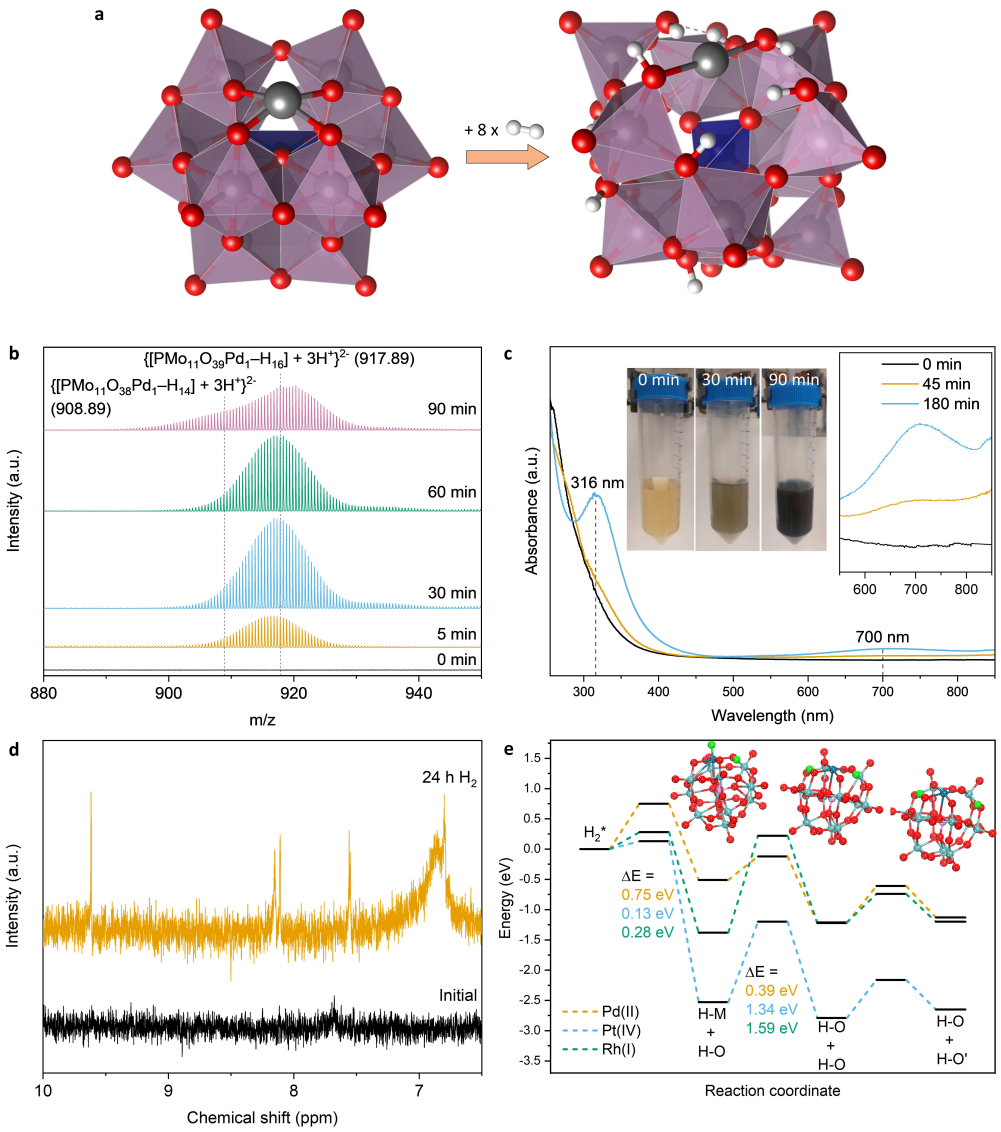

Figure 1. Structure of $PMo_{11}O_{39}Pd_1$ after hydrogen spillover. a) Catalyst structure before and after full hydrogen spillover (16 H atoms) based on DFT calculations. Color code—grey: Pd, pink: Mo, blue: P, red: O, white: H. b) ESI-MS of $PMo_{11}O_{39}Pd_1$ during the hydrogen spillover for different durations. Some of the higher *m/z* species occur due to Na^+ and K^+ adducts. c) UV/Vis spectroscopy of $PMo_{11}O_{39}Pd_1$ during the hydrogen spillover (45 and 180 min), photographs of the solution at different time points are shown in the inset. d) ^1H NMR of $PMo_{11}O_{39}Pd_1$ before and after 24 h hydrogen spillover. e) DFT-calculated reaction energies of the heterolytic H_2 dissociation and subsequent spillover on adjacent (H–O) as well as distant sites (H–O′) for different $PMo_{11}O_{39}M_1$ catalysts (detailed structures are shown in Figure S16). Color code – grey: Pd, light blue: Mo, pink: P, red: O, green: H.

characterization such as probe molecule DRIFTS and XPS among others.

CO DRIFTS suggests that all materials comprise positively charged metal ions for all three $PMo_{11}O_{39}M_1$ materials, with CO vibrations for Pd at 2113 cm^{-1} (consistent with partially positive $Pd^{\delta+}$),[13] for Pt at 2105 cm^{-1} (suggestive of Pt^{4+}),[14] and for Rh at 2109, 2072, 2024, and 1993 cm^{-1} (likely due symmetric and asymmetric vibrations of a mixture of Rh^{+} and Rh^{3+}),[10b,15] respectively (Figure S3b). This reduction of Rh^{3+} in situ during CO exposure is relatively common and single Rh atoms on Mo-based POMs can be reduced to Rh^{+} rapidly at room temperature.[10b] None of the materials exhibit broad CO vibrations below 1950 cm^{-1}, which would be indicative of bridged site CO on metal nanoclusters or -particles. We therefore conclude that despite small differences in the oxidation states, the different $PMo_{11}O_{39}M_1$ materials are comprised of the same structural motifs merely differing by the identity of their metal active sites. CO DRIFTS further shows the stability of the atomic dispersion of Pd on $PMo_{11}O_{39}Pd_1$ even after hydrogen spillover treatment (Figure S3c) providing further evidence that hydrogen spillover indeed occurs over atomically dispersed metal sites.

Infrared spectroscopy suggested high purity of the $PMo_{11}O_{39}M_1$ samples after precipitation (Figure S4). When $PMo_{11}O_{39}Pd_1$ was exposed to H_2 at room temperature, a gradual color change from yellow to blue was observed. ESI-MS of the solution after color change suggested the formation of catalyst species containing spilled over hydrogen. The m/z values of the catalyst after H_2 exposure for 60 min were consistent with the formation of $\{[PMo_{11}O_{39}Pd_1\text{-}H_{16}]+3H^+\}^{2-}$ (calc.: 917.89, expt.: 917.86) with 16 spilled over H atoms on the POM (Figure 1b and Figure S5). We did not observe any species with higher H coverage suggesting that this is the highest hydrogen spillover state of $PMo_{11}O_{39}Pd_1$ under our reaction conditions. The lack of color changes and unaltered ESI-MS spectra of $PMo_{11}O_{39}$, $PW_{11}O_{39}Pd_1$, $PMo_{11}O_{39}Rh_1$, and $PMo_{11}O_{39}Pt_1$ after H_2 exposure revealed that none of those exhibit a similar behavior suggesting that the combination of Mo-based POMs and Pd is unique (Figure S6). UV/Vis spectroscopy of the Pd-Mo POM system showed the formation of two distinct states with absorption maxima at 700 and 316 nm, respectively (Figure 1c). This indicates significant changes in the electronic state of the POM-based SAC as should be expected from the oxidation state change of Mo. Reduction of Mo^{VI} to Mo^{V} often leads to absorption at 600–800 nm[16] while more significant reduction of the POM changes the color to a deep blue in this case with the absorption maximum in the UV region.[17] The occurrence of two distinct maxima observed by UV/Vis spectroscopy implies the formation of two sets of species during hydrogen spillover (Figure 1c). ESI-MS at different times of H_2 exposure further supports the notion that distinct states of hydrogen spillover exist with a group of intermediate species (plausibly ranging from 8 to 12 or 14 H atoms) centered at around $\{[PMo_{11}O_{39}Pd_1\text{-}H_{12}]+3H^+\}^{2-}$ (calc.: 915.88, expt.: 915.84) (Figure 1b and Figures S5 and S7), before reaching the saturated state of $[PMo_{11}O_{39}Pd_1\text{-}H_{16}]$. ^{1}H NMR of the catalyst before and after 24 h H_2 exposure in d^6-DMSO showed well-resolved and sharp resonances of spilled over H. The strong downfield shift of the ^{1}H NMR signals highlight the electron-deficient nature of the spilled over H which thus should be viewed as protons on the reduced $PMo_{11}O_{39}Pd_1$ supported by a Bader charge analysis of the components of $PMo_{11}O_{39}Pd_1$ at different H coverages (Figure 1d, Figure S8, and Table S1). Integrated ratios between the ^{1}H resonances (1:1:1:1) corroborate the formation of $[PMo_{11}O_{39}Pd_1\text{-}H_{16}]$ as identified by ESI-MS. Solvents appeared to exert a drastic effect on hydrogen spillover kinetics with a general promoting role of polar protic solvents (Figures S9 and S10). This would suggest that proton transfer is important for hydrogen spillover or that apolar solvents destabilize the transition or final state of the catalyst during or after H transfer. This is consistent with the generally assumed critical role of water, even when merely present as adlayers in gas phase catalyst systems, on hydrogen spillover.[9,18] We further evaluated the stability of Pd sites against sintering by XPS and CO DRIFTS after H_2 treatment under different conditions (Figures S3 and S11).

From the observations mentioned above, we propose two subsequent steps to occur with $PMo_{11}O_{39}Pd_1$ during H_2 exposure:

$$PMo_{11}O_{39}Pd_1 + x/2\,H_2 \rightarrow PMo_{11}O_{39}Pd_1\text{-}H_x \quad (8 \le x \le 14,\ \text{intermediate state}) \tag{1}$$

$$PMo_{11}O_{39}Pd_1\text{-}H_x + (16-x)/2\,H_2 \rightarrow PMo_{11}O_{39}Pd_1\text{-}H_{16} \quad (\text{full H coverage}) \tag{2}$$

From the ESI-MS analysis of the hydrogen spillover process after elongated times (90 min or longer), the formation of an oxygen vacancy from $\{[PMo_{11}O_{39}Pd_1\text{-}H_{16}]+3H^+\}^{2-}$ started to occur as evidenced by a mass loss of one molecule of water (Figure 1b). This was corroborated by the fragmentation of the $\{[PMo_{11}O_{39}Pd_1\text{-}H_{16}]+3H^+\}^{2-}$ showing the formation of $\{[PMo_{11}O_{38}Pd_1\text{-}H_{14}]+3H^+\}^{2-}$ (Figure S12).

$$PMo_{11}O_{39}Pd_1\text{-}H_{16} \rightarrow PMo_{11}O_{38}Pd_1\text{-}H_{14} + H_2O \tag{3}$$

As reported previously, oxygen vacancies are closely linked to hydrogenation/deoxygenation reactions (see below).[19] For the NBu_4-precipitated solid-state material, we detected EPR-active Mo^{V} suggesting that those are intermediates in the hydrogen spillover process (Figure S13). The EPR signal is only seen in the solid state probably due to the high reactivity of Mo^{V} in the presence of water or magnetic coupling of Mo^{V} rendering them EPR silent.[20] XPS on the solid-state $PMo_{11}O_{39}Pd_1$ compound further provided evidence that the majority of Mo^{VI} is reduced after H_2 exposure (Figure S11). Within a few hours' exposure to air, hydrogen spillover on $PMo_{11}O_{39}Pd_1$ was completely reversible but stable under a flow of inert gas for 20 h (Figures S14 and S15). This suggests that spillover is not spontaneously reversible but spilled over H is capable of reacting with oxidants such as O_2.

DFT calculations were employed to identify why the combination of $PMo_{11}O_{39}$ and Pd is special for hydrogen

spillover. Complexes between the lacunary POM and Pd^{II}, Pt^{IV}, and Rh^{I} (Figure S16) were considered in line with the oxidation states we observed based on CO DRIFTS. For all catalysts, only the heterolytic splitting of H_2 into metal-based $H^{\delta-}$ and POM-based $H^{\delta+}$ were feasible mechanisms. Pd^{II} exhibited the highest H_2 dissociation barriers, while Pt^{IV} and Rh^{I} split H_2 with negligible barriers (Figure 1e) which seems to be in contrast with experimental observations. For hydrogen spillover to occur, however, the subsequent transfer of H from the metal site to the support needs to be considered as well. Pd^{II} demonstrated the lowest barriers, whereas activation energies were >1.5 eV for Pt^{IV} and Rh^{I}, rendering them kinetically incompetent for H spillover at room temperature. Hydrogen diffusion barriers between O atoms on the support were low (≈ 0.5 eV) and only marginally affected by the single metal cation (Figure 1e). The hydrogen spillover capacity of $PMo_{11}O_{39}Pd_1$ was investigated by obtaining the average hydrogen adsorption energy relative to H_2 gas as a function of H coverage (Figures S17 and S18). Consistent with experimental data, 16 H atoms appear to be the approximate limit upon which further H spillover becomes endergonic, suggesting that the experimentally observed maximum H coverage is determined by thermodynamic rather than kinetic limitations. Those results support our observations that metal-POM combinations other than $PMo_{11}O_{39}Pd_1$ do not show hydrogen spillover as well as the catalyst:H ratios after hydrogen spillover based on ESI-MS and ^{1}H NMR. DFT calculations further investigated the impact of POM composition on the H_2 splitting behavior suggesting that spillover is thermodynamically rather than kinetically limited on $PW_{11}O_{39}Pd_1$ as compared to $PMo_{11}O_{39}Pd_1$ (Figure S19). Although hydrogen spillover from metallic Pt to various reducible supports is commonly assumed, previous experiments also suggested that cationic Pt behaves differently from its metallic counterpart.[3a,b,6a]

The distinction of two related spillover species by UV/Vis provides us with a direct and non-destructive tool to follow hydrogen spillover kinetics. The formation of the first set of stable spillover intermediates with its UV/Vis absorbance at 700 nm has a positive order towards H_2 concentration (1.52) confirming that H is involved in the rate-determining step and that spillover entails multiple elementary steps (Figure 2a). We further observed a negative order towards the concentration of $PMo_{11}O_{39}Pd_1$ (-0.99) (Figure 2b). With this, the apparent activation enthalpy and entropy were determined to be $55.2 (\pm 1.7)$ kJ mol^{-1} and $-133.5 (\pm 7.8)$ J mol^{-1} K^{-1}, respectively (Figure 2c). Hydrogen spillover overall as defined in Equation (1) is an entropically disfavored process and thus it is reasonable to assume that the apparent activation entropy is negative.

The absence of H spillover intermediates with low H coverages (i.e. below approximately 8 H, Figure 1b) suggests a level of autocatalytic hydrogen spillover. A DFT analysis of the impact of H coverage on the H_2 splitting barriers reveals a continuous decrease in the H_2 activation barrier on $PMo_{11}O_{39}Pd_1$ as hydrogen spillover progresses (Figure S20). Based on DFT calculations, the hydrogen splitting mechanism also changes from heterolytic to homolytic H–H cleavage with higher H coverage. At a coverage of around 14 H atoms, the activation barriers for H_2 splitting become almost negligible and thus we may assume that the rate-determining step changes from H_2 splitting to the diffusion of H on the support. Yang et al. for example have shown previously that the diffusivity of H on spillover catalysts is inversely proportional to the extent of hydrogen coverage.[21] Those two competing effects might lead to the observation of only a few distinct hydrogen spillover intermediates. Overall, an important finding here is that the initial spillover of hydrogen benefits the subsequent activation and spillover of H, i.e., it is a self-catalytic process, which is consistent with the occurrence of an induction period that is sometimes observed for hydrogen spillover.[6a]

To identify the relation of hydrogen spillover to catalysis, we tested the nitrobenzene (NB) hydrogenation during H_2 exposure of the catalyst. We found NB conversion to increase in an accelerated manner with time (Figure 3a) with the reaction rate acceleration following an approximately two-stage linear behavior with constants of 0.040 and 0.263 min^{-2}, respectively (Figure 3b). The inflection point of this increase at around 40 mins coincides with the onset formation of the final hydrogen spillover species (that is $PMo_{11}O_{39}Pd_1$-H_{16}). We therefore conclude that spilled over H on the catalyst has a unique reactivity in the hydrogenation of NB. In order to test this hypothesis, we resorted to the selective poisoning of Pd species by benzyl

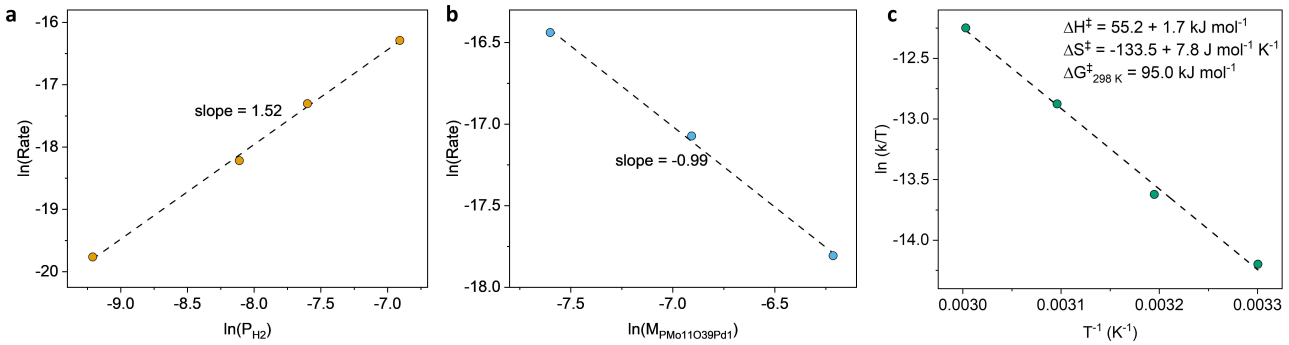

Figure 2. Kinetics of the hydrogen spillover on $PMo_{11}O_{39}Pd_1$. Reaction orders towards a) H_2 and b) $PMo_{11}O_{39}Pd_1$, during the hydrogen spillover process. c) Eyring plot for the first hydrogen spillover step with the absorbance at 700 nm.

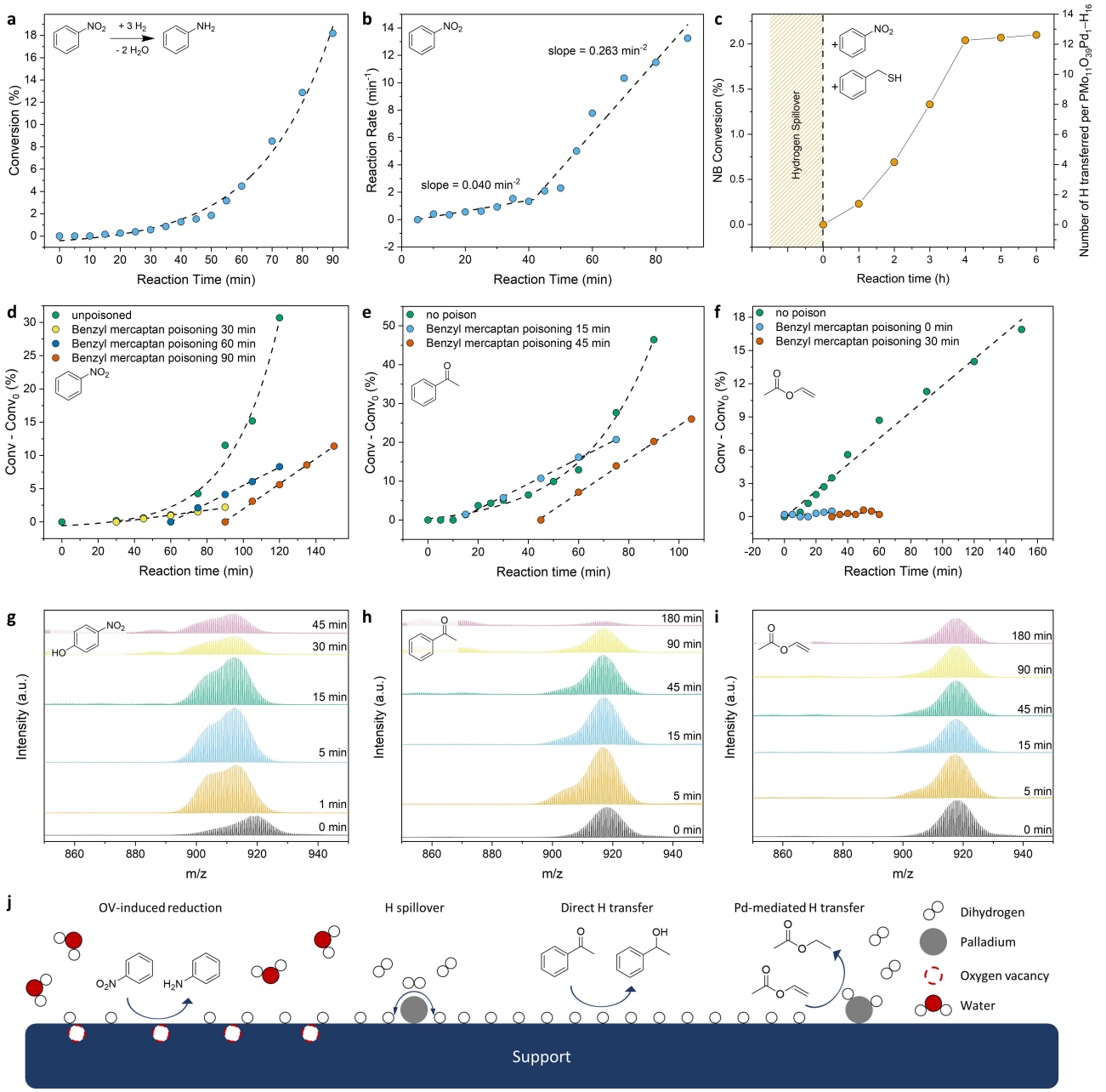

Figure 3. Hydrogenation kinetics and poisoning studies. a) Conversion and b) reaction rates for the NB hydrogenation during the hydrogen spillover. The slopes (reaction rate acceleration constants in min^{-2}) are indicated as slopes of the plot. c) Long-term poisoning study of $PMo_{11}O_{39}Pd_1$ during the NB hydrogenation reaction with 100 equivalents of substrate (details on how the number of H transfer is calculated are in the experimental section). Reaction kinetics for the hydrogenation of d) NB, e) ACP, f) VA with the addition of 2 equivalents benzyl mercaptan after different reaction times. g–i) ESI-MS during the reaction between $\{[PMo_{11}O_{39}Pd_1\text{-}H_{16}]+3\,H^+\}^{2-}$ and different substrates. $PMo_{11}O_{39}Pd_1$ was subjected to H_2 for 120 min prior to the addition of 25 equivalents of substrate. g) NP, h) ACP, i) VA, j) Schematic depiction of the contribution of spilled over H to hydrogenation catalysis for different substrates. Reaction conditions for d–i) $V=0.02$ L, $C_{PMo11O39}=1$, 0.25 (c) mmol L^{-1}, $C_{Pd}=0.33$, 0.08 (c) mmol L^{-1}, F (5 % H_2) = 40 $cm^3\,min^{-1}$, T = RT (a–d, g–i), 40 (e), or 0 (f) °C, $C_{substrate}=8.25$ mmol L^{-1} with the addition of benzyl mercaptan to $C_{mercaptan}=0.66$, 0.17 (c) mM after different reaction times ranging from 0 to 90 min. Conversions in d–f were plotted as difference between conversion and conversion at $t=0$—the time point when poison was added.

mercaptan, a thiol with strong affinity to soft Lewis acids like Pd^{2+}. Adding two equivalents (relative to Pd) of benzyl mercaptan to $\{[PMo_{11}O_{39}Pd_1\text{-}H_{16}]+3\,H^+\}^{2-}$ after 120 min hydrogen spillover together with the substrate NB in large excess shows that the poisoning protocol is indeed effective in preventing further hydrogen activation and spillover to the support. Even with the poison present, two NB molecules were converted to aniline per POM equating to the total transfer of 12 H atoms per $PMo_{11}O_{39}Pd_1$ unit to the substrate within 240 min (Figure 3c, details on the calcula-

tion of the number of H transferred are in the experimental section). Reaction rates and their changes were further elucidated during catalysis with catalyst poisoning at different time points. Again, for the hydrogenation of NB the conversion increased exponentially without poison while following a strict linear increase after adding benzyl mercaptan. The correlated reaction rates are thus increasing linearly for the unpoisoned case while they stayed constant for the case where the poison was added. Noticeably, the reaction rates were dependent on the time point of benzyl mercaptan addition indicating that the extent of spillover affects reaction kinetics (Figure 3d and Figure S21a). We observed similar trends for the hydrogenation of acetophenone (ACP) with increasing or constant reaction rates when no or two equivalents of benzyl mercaptan were added, respectively (Figure 3e and Figure S21b). For the hydrogenation of vinyl acetate (VA) comprising an unsaturated C=C bond the conversion increased linearly with time with the related reaction rates thus being constant. Upon addition of benzyl mercaptan, the conversion of VA did not increase anymore with reaction rates immediately dropping to zero (Figure 3f and Figure S21c). This strongly suggests that spilled over H did not participate in the hydrogenation of C=C bonds but instead that H transfer occurred from the Pd site. Overall, there seems to be a strong tendency of the hydrogenation of polar functional groups by spilled over H while less polar bonds rely on the transfer of H directly from metal active sites.

ESI-MS was used to shed further light on the participation of spilled over H in the hydrogenation reaction of different substrates. When substrates were added to the catalyst after hydrogen spillover for 120 min, clear differences were observed among them. For VA, there was no obvious change in the composition of the spilled over catalyst structure within 180 min (Figure 3i), confirming that spilled over H does not participate in C=C bond hydrogenation. For ACP, the intensity of the mass peak for $\{[PMo_{11}O_{39}Pd_1\text{-}H_{16}]+3H^+\}^{2-}$ decreased significantly over time with almost complete H removal after 180 min (Figure 3h). This is consistent with the contribution of spilled over H to the hydrogenation of C=O bonds. The biggest differences arise for the hydrogenation of nitrophenol (NP, NP is used to replace NB for its higher solubility in water) with the immediate removal of H from the support and the formation of the oxygen vacant species $\{[PMo_{11}O_{38}Pd_1\text{-}H_4]+3H^+\}^{2-}$ (Figure 3g). The formation of this intermediate was additionally confirmed by hydrogen spillover experiments in the presence of NP (Figures S22 and S23), while the H transfer stoichiometry was consistent with the transfer of 12 H atoms per $PMo_{11}O_{39}Pd_1\text{-}H_{16}$ discussed earlier (Figure 3c). Fragmentation of the NP-containing intermediate confirmed the ability of the substrate to refill the oxygen vacancy during reaction (Figure S24). These ESI-MS experiments support the notion that spilled over H is responsible for the hydrogenation of certain reducible bonds while the exact nature of participation of these H atoms differs in mechanism between different functional groups (e.g. the direct transfer of H, formation of oxygen vacancies, etc., Figure 3j). Those findings were further corroborated by measuring the concentration of hydrogen spillover species by UV/Vis in the presence of the three reducible substrates (Figure S25) as well as the observation that the hydrogen spillover species can be completely recovered after all reducible substrate was consumed (Figure S26).

We measured the initial hydrogenation turnover frequencies for NB and VA with $PMo_{11}O_{39}Pd_1$ after different times of H_2 exposure to obtain a clearer correlation between the extent of hydrogen spillover and the hydrogenation kinetics. A 33-fold increase in NB hydrogenation activity after 90 min initial hydrogen exposure was observed (Figure 4b) consistent with proceeding H spillover and oxygen vacancy formation. In contrast, the reaction rate dropped by a factor of 3.3 after 90 min H_2 exposure of the catalyst for VA hydrogenation (Figure 4a). This indicates that not only does hydrogen spillover contribute to the hydrogenation of various reducible groups differently, but hydrogen spillover can also be detrimental to catalysis in certain cases.

Since experimental data provide good indication that hydrogenation may occur either on the POM support through spilled over hydrogen or on the metal site through Pd-mediated hydrogen transfer, the reaction energies of the VA and ACP hydrogenation over two types of sites located on the support and on Pd under different hydrogen coverages were calculated by DFT. For the hydrogenation of VA, only the Pd site showed reasonably low reaction barriers with marked effects of the H coverage on both kinetics and thermodynamics of the reaction. Activation energies were calculated to be 0.07 eV and 0.33 eV for low and high H coverages, respectively (Figure 4c and Figures S27 and S28). In contrast, the hydrogenation of polar bonds such as C=O in ACP only proceeds with low activation barriers when $PMo_{11}O_{39}Pd_1$ exhibits high H coverages. Low hydrogen coverages increase the reaction barriers and render the hydrogenation far less exothermic (Figure 4d and Figures S29, S30, and S31). In addition, the local H density, depending on the specific location of H atoms, significantly impacted the hydrogenation reaction barriers (Figure S32). The hydrogenation of NB should be assumed to depend on the extent of hydrogen spillover as well, since the proclivity for forming oxygen vacancies is H coverage-dependent (Table S2). Those findings are consistent with experiments suggesting that different sites on Pt/TiO_2 might be involved in the hydrogenation of functional groups of differing polarity.[22] Kinetic barriers for the deoxygenation of ACP are high on Mo POM-based Pd SACs, in accordance with the lack of experimentally observed ethylbenzene as well one of our previous studies (Figure S33).[23] While for the above-mentioned three reactions, we did not observe differences in the H-coverage-dependent selectivity, analogous reactions with cinnamaldehyde suggest that the activity for C=O bond hydrogenation of $PMo_{11}O_{39}Pd_1$ is approximately 12 times higher after hydrogen spillover compared to the catalyst without any pre-treatment (Figure S34). We may ascribe those differences in reactivity to the change in oxidation state of Pd, as reflected by a shift in XPS binding energies of Pd from initially 337.6 eV to 337.1 eV as hydrogen spillover progressed (Figure S11), as well as by Bader charge analysis of $PMo_{11}O_{39}Pd_1$ as a function of H coverage

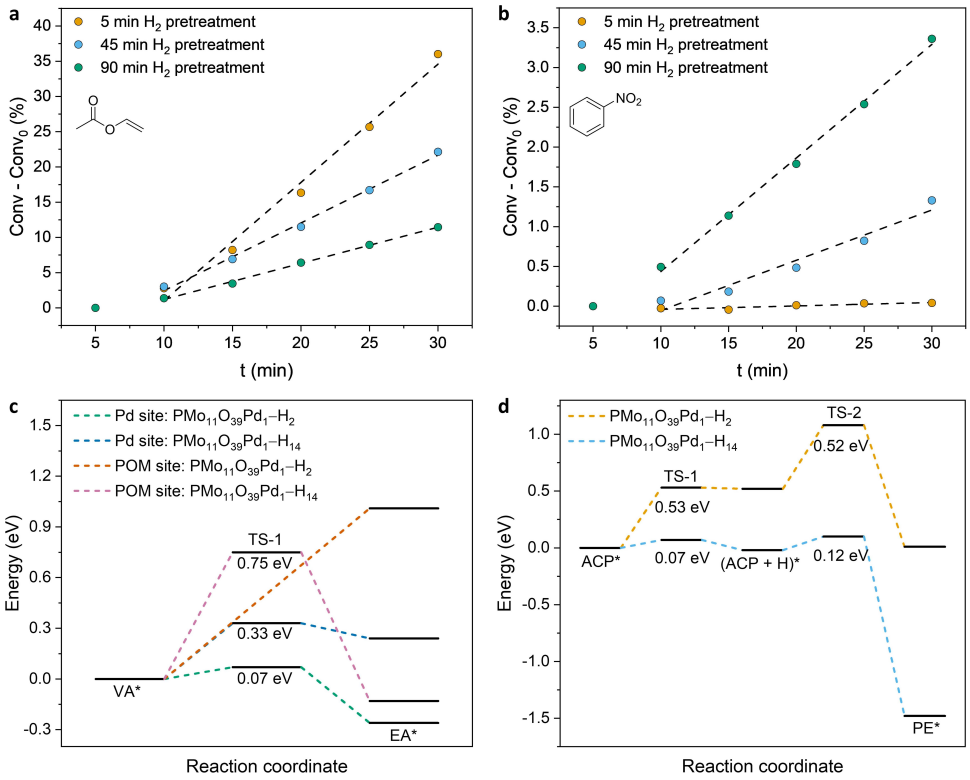

Figure 4. Correlation between the hydrogen spillover and the hydrogenation activity. Substrate conversion for the a) VA and b) NB hydrogenation after hydrogen spillover for 5, 45, or 90 min. DFT calculated reaction energies for the c) VA and d) ACP hydrogenation for different sites on the catalyst and H coverages. EA stands for ethyl acetate, the hydrogenation product of VA; PE stands for 1-phenylethanol, the hydrogenation product of ACP.

(Table S1). This reactivity trend is consistent with previous reports on the drop in C=C bond hydrogenation activity when the oxidation state of Pd was reduced.[24] We further found that a catalyst not exhibiting hydrogen spillover ($PW_{11}O_{39}Pd_1$) was significantly more active in the hydrogenation of vinyl acetate (Figure S35).

To identify whether the findings related to hydrogen spillover are specific to POM-supported SACs or can also be applied to more traditional nanoparticle-based catalysts, we performed analogous investigations on the archetypical hydrogen spillover catalyst Pt/WO_3, which we observed to also undergo a color change from yellow to blue during H_2 exposure (Figure S36). This color change was concomitant with the formation of Pt particles with diameters on the order of 3–5 nm (Figure S37) while the absence of metal leaching into solution was confirmed by ICP-OES (Table S3). Plotting the initial reaction rates for the VA and ACP hydrogenation reaction against time after different durations of H_2 treatment revealed a picture comparable to the case of $PMo_{11}O_{39}Pd_1$. Hydrogenation rates dropped by a factor of 7.8 for VA when Pt/WO_3 was exposed to H_2 for 90 min while the opposite was true for NB with a rate increase by a factor of 3.6 (Figures 5a,b). We therefore again conclude that spilled over H positively contributes to NB reduction while hindering VA hydrogenation. Further verification of this hypothesis was obtained from isotope labelling experiments. Provided that the spilled over H exchanges protons with protic solvents and considering that the rate of hydrogen spillover is considerably larger than its reversal (which we found to be true for $PMo_{11}O_{39}Pd_1$), differences in the D incorporation should be expected when D_2O and H_2 are used during the hydrogenation reaction. Indeed, significant deuteration of the ACP hydrogenation product 1-phenylethanol was observed while the D incorporation was negligible when VA was used as substrate (Figures 5c,d). This strongly supports the notion that H/D from the support is involved in the hydrogenation of the polar C=O bond while only H from the Pt nanoparticles are transferred to VA.

Studies on bimetallic single-atom alloys have revealed certain factors affecting spillover catalysis but the nature of H on metallic surfaces is very different compared to more conventionally investigated metal oxides.[3c,25] Understanding the impact of hydrogen spillover on the electronic structure of the catalyst as well as its hydrogenation activity might have implications for reactions that do not involve H atom transfer directly but which may either form H species as side-product or benefit from the co-feeding of H_2 such as shown recently for epoxidation reactions.[26] For reactions like the CO_2 or N_2 hydrogenation, the contribution of hydrogen spillover to catalysis has been discussed very recently and remains inconclusive.[27] Based on our results, it is very likely that hydrogen spillover plays a crucial role in forming oxygen vacancies and transferring H to polar

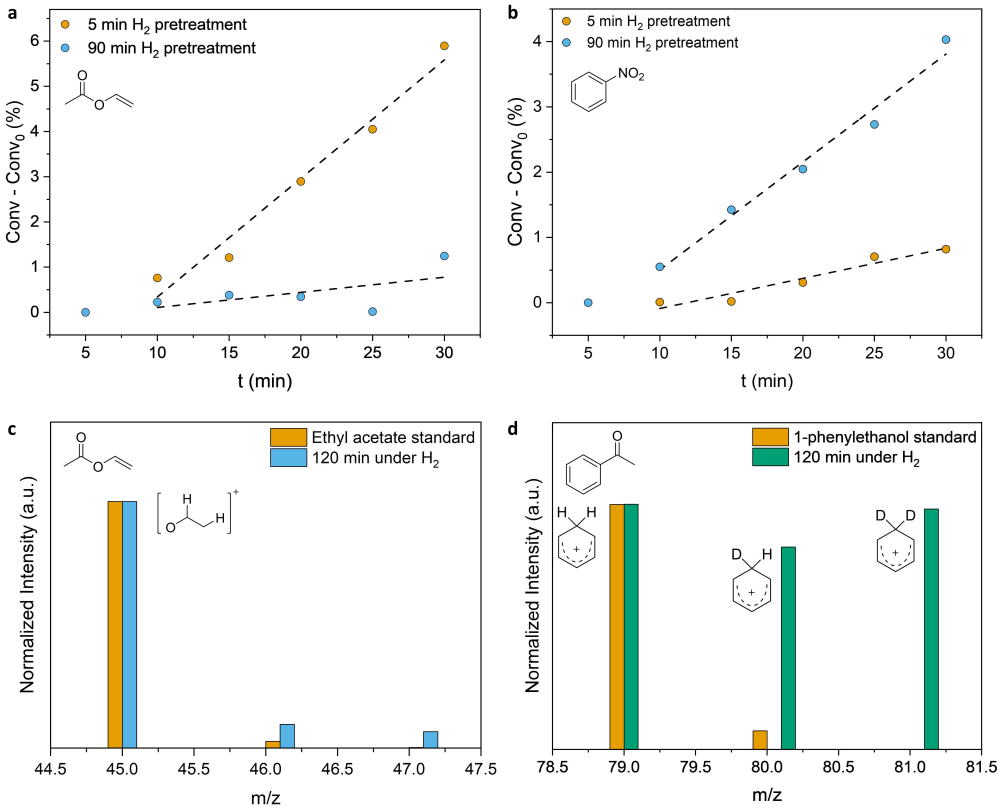

Figure 5. Correlation between hydrogen spillover and the hydrogenation activity on Pt/WO_3. Substrate conversion for the hydrogenation of a) VA and b) NB after hydrogen spillover for 5 or 90 min. Deuterium isotope-labelling during the hydrogenation of c) VA and d) ACP in D_2O as solvent after treatment with H_2 as reductant for 120 min. The MS spectra of standard samples of the reaction products are shown for comparison.

molecules like CO_2. Caution should be exercised for correlating hydrogen spillover and enhanced catalytic activity since in some cases limiting the spillover of H on the support appears to be beneficial. As a corollary to that, hydrogen spillover obviously affects the selectivity in the hydrogenation of different functional groups and once fully understood could offer an additional handle to rationally design hydrogenation catalysts. We developed a related heterogeneous single-atom catalyst and observed comparable hydrogen spillover behavior as well as hydrogenation kinetics for solid–gas biphasic processes and we expect those data to shed further light on the curious case of hydrogen spillover.

Conclusion

In summary, the unique soluble SAC-POM catalyst system allows for the investigation of hydrogen spillover to a previously unattainable level of detail. Our observations based on kinetics, spectroscopy, spectrometry, and DFT calculations reveal that hydrogen spillover is an autocatalytic process, that the spilled over H on metal oxides is highly protonic in nature and induce vacancy formation on the support, with the maximum H coverage determined by thermodynamic limitations. The nature of the contribution of spilled over H to catalysis depends on the reducible functional group: for nitro group and C=O bond hydrogenation spilled over hydrogen enhances the reaction rate by direct participation from the support and may additionally decrease the reaction barrier on the metal site; for C=C bond hydrogenation, in stark contrast, spilled over hydrogen cannot be directly added to the double bond while their presence increases the hydrogenation barrier on the metal site, thus slowing down the reaction. Comparable experiments performed on Pt/WO_3 support the notion that some of the conclusions in particular pertaining to the contribution of spilled over H to catalysis drawn from the POM-based SAC are applicable for other catalysts as well. This study provides fundamental insights as well as guidance for designing improved hydrogenation catalysts targeted for various substrates. It may also inspire more studies of complex catalytic phenomena on model catalyst systems comprising single-atom sites.[11a,28] We envision that this platform can be utilized more extensively in the future to resolve long-standing questions in the fields of catalysis and beyond.

Acknowledgements

M.J.H. acknowledges the SINGA scholarship for financing his PhD studies. Part of this work was performed at the Center for Nanophase Materials Sciences, a US Department

of Energy Office of Science User Facility. We thank Dr. Yao Xu and Prof. Ding Ma for help with XPS measurements.

Conflict of Interest

The authors declare no conflict of interest.

Data Availability Statement

The data that support the findings of this study are available from the corresponding author upon reasonable request.

Keywords: Mass Spectrometry · Polyoxometalates · Reaction Kinetics · Single-Site Catalysis · Structure–Activity Correlations

[1] R. Prins, *Chem. Rev.* **2012**, *112*, 2714–2738.
[2] U. Roland, T. Braunschweig, F. Roessner, *J. Mol. Catal. A* **1997**, *127*, 61–84.
[3] a) N. Doudin, S. F. Yuk, M. D. Marcinkowski, M.-T. Nguyen, J.-C. Liu, Y. Wang, Z. Novotny, B. D. Kay, J. Li, V.-A. Glezakou, G. Parkinson, R. Rousseau, Z. Dohnálek, *ACS Catal.* **2019**, *9*, 7876–7887; b) J. Liu, A. J. R. Hensley, G. Giannakakis, A. J. Therrien, A. Sukkar, A. C. Schilling, K. Groden, N. Ulumuddin, R. T. Hannagan, M. Ouyan, M. Flytzani-Stephanopoulos, J. S. McEwen, E. C. H. Sykes, *Appl. Catal. B* **2021**, *284*, 119716; c) L. Jiang, K. Liu, S.-F. Hung, L. Zhou, R. Qin, Q. Zhang, P. Liu, L. Gu, H. M. Chen, G. Fu, N. Zheng, *Nat. Nanotechnol.* **2020**, *15*, 848–853.
[4] V. Fung, G. Hu, Z. Wu, D.-e. Jiang, *J. Phys. Chem. Lett.* **2020**, *11*, 7049–7057.
[5] J. Im, H. Shin, H. Jang, H. Kim, M. Choi, *Nat. Commun.* **2014**, *5*, 3370.
[6] a) P. A. Sermon, G. C. Bond, *J. Chem. Soc. Faraday Trans. 1* **1976**, *72*, 730–744; b) P. A. Sermon, G. C. Bond, *J. Chem. Soc. Faraday Trans. 1* **1976**, *72*, 745–754.
[7] P. C. H. Mitchell, A. J. Ramirez-Cuesta, S. F. Parker, J. Tomkinson, D. Thompsett, *J. Phys. Chem. B* **2003**, *107*, 6838–6845.
[8] Y. Lykhach, T. Staudt, M. Vorokhta, T. Skála, V. Johánek, K. C. Prince, V. Matolín, J. Libuda, *J. Catal.* **2012**, *285*, 6–9.
[9] W. Karim, C. Spreafico, A. Kleibert, J. Gobrecht, J. Vande-Vondele, Y. Ekinci, J. A. van Bokhoven, *Nature* **2017**, *541*, 68–71.
[10] a) B. Zhang, H. Asakura, J. Zhang, J. Zhang, S. De, N. Yan, *Angew. Chem. Int. Ed.* **2016**, *55*, 8319–8323; *Angew. Chem.* **2016**, *128*, 8459–8463; b) M. J. Hülsey, B. Zhang, Z. Ma, H. Asakura, D. A. Do, W. Chen, T. Tanaka, P. Zhang, Z. Wu, N. Yan, *Nat. Commun.* **2019**, *10*, 1330; c) B. Zhang, G. Sun, S. Ding, H. Asakura, J. Zhang, P. Sautet, N. Yan, *J. Am. Chem. Soc.* **2019**, *141*, 8185–8197; d) M. J. Hülsey, G. Sun, P. Sautet, N. Yan, *Angew. Chem. Int. Ed.* **2021**, *60*, 4764–4773; *Angew. Chem.* **2021**, *133*, 4814–4823; e) M. J. Hülsey, S. Baskaran, S. Ding, S. Wang, H. Asakura, S. Furukawa, S. Xi, Q. Yu, C.-Q. Xu, J. Li, N. Yan, *CCS Chem.* **2022**, DOI 10.31635/ccschem.022.202201914.
[11] a) R. Liu, C. Streb, *Adv. Energy Mater.* **2021**, *11*, 2101120; b) P. Yang, U. Kortz, *Acc. Chem. Res.* **2018**, *51*, 1599–1608; c) B. Rausch, M. D. Symes, G. Chisholm, L. Cronin, *Science* **2014**, *345*, 1326–1330.
[12] a) V. Artero, D. Laurencin, R. Villanneau, R. Thouvenot, P. Herson, P. Gouzerh, A. Proust, *Inorg. Chem.* **2005**, *44*, 2826–2835; b) R. Copping, A. J. Gaunt, I. May, M. J. Sarsfield, D. Collison, M. Helliwell, I. S. Denniss, D. C. Apperley, *Dalton Trans.* **2005**, 1256–1262.
[13] a) D. Jiang, G. Wan, C. E. García-Vargas, L. Li, X. I. Pereira-Hernández, C. Wang, Y. Wang, *ACS Catal.* **2020**, *10*, 11356–11364; b) C.-T. Kuo, Y. Lu, P. Arab, K. S. Weeraratne, H. El-Kaderi, A. M. Karim, *Cell Rep. Phys. Sci.* **2021**, *2*, 100495; c) M. Piernavieja-Hermida, Z. Lu, A. White, K.-B. Low, T. Wu, J. W. Elam, Z. Wu, Y. Lei, *Nanoscale* **2016**, *8*, 15348–15356.
[14] a) S. Ding, Y. Guo, M. J. Hülsey, B. Zhang, H. Asakura, L. Liu, Y. Han, M. Gao, J.-y. Hasegawa, B. Qiao, T. Zhang, N. Yan, *Chem* **2019**, *5*, 3207–3219; b) X. I. Pereira-Hernández, A. DeLaRiva, V. Muravev, D. Kunwar, H. Xiong, B. Sudduth, M. Engelhard, L. Kovarik, E. J. M. Hensen, Y. Wang, A. K. Datye, *Nat. Commun.* **2019**, *10*, 1358; c) H. Jeong, D. Shin, B.-S. Kim, J. Bae, S. Shin, C. Choe, J. W. Han, H. Lee, *Angew. Chem. Int. Ed.* **2020**, *59*, 20691–20696; *Angew. Chem.* **2020**, *132*, 20872–20877.
[15] S. Ding, M. J. Hülsey, H. An, Q. He, H. Asakura, M. Gao, J.-y. Hasegawa, T. Tanaka, N. Yan, *CCS Chem.* **2021**, *3*, 1814–1822.
[16] a) J. Chen, S. Liu, W. Feng, G. Zhang, F. Yang, *Phys. Chem. Chem. Phys.* **2013**, *15*, 5664–5669; b) S. Ohisa, K. Endo, K. Kasuga, M. Suzuki, T. Chiba, Y.-J. Pu, J. Kido, *Inorg. Chem.* **2018**, *57*, 1950–1957; c) M. Dudek, A. Samotus, *Transition Met. Chem.* **1985**, *10*, 271–274.
[17] H. Oku, N. Ueyama, M. Kondo, A. Nakamura, *Inorg. Chem.* **1994**, *33*, 209–216.
[18] a) J. E. Benson, H. W. Kohn, M. Boudart, *J. Catal.* **1966**, *5*, 307–313; b) R. B. Levy, M. Boudart, *J. Catal.* **1974**, *32*, 304–314.
[19] a) K. A. Goulas, A. V. Mironenko, G. R. Jenness, T. Mazal, D. G. Vlachos, *Nat. Catal.* **2019**, *2*, 269–276; b) J. Fu, J. Lym, W. Zheng, K. Alexopoulos, A. V. Mironenko, N. Li, J. A. Boscoboinik, D. Su, R. T. Weber, D. G. Vlachos, *Nat. Catal.* **2020**, *3*, 446–453.
[20] W. Gruenert, A. Y. Stakheev, R. Feldhaus, K. Anders, E. S. Shpiro, K. M. Minachev, *J. Phys. Chem.* **1991**, *95*, 1323–1328.
[21] Y. Li, F. H. Yang, R. T. Yang, *J. Phys. Chem. C* **2007**, *111*, 3405–3411.
[22] a) L. R. Baker, G. Kennedy, M. Van Spronsen, A. Hervier, X. Cai, S. Chen, L.-W. Wang, G. A. Somorjai, *J. Am. Chem. Soc.* **2012**, *134*, 14208–14216; b) G. Kennedy, L. R. Baker, G. A. Somorjai, *Angew. Chem. Int. Ed.* **2014**, *53*, 3405–3408; *Angew. Chem.* **2014**, *126*, 3473–3476; c) G. Kennedy, G. Melaet, H.-L. Han, W. T. Ralston, G. A. Somorjai, *ACS Catal.* **2016**, *6*, 7140–7147.
[23] M. J. Hülsey, S. Geng, Z. Bin, X. Yao, D. Shipeng, W. Sie Shing, Z. Ying, F. Shinya, A. Hiroyuki, C. Yongqiang, W. Zili, S. Rui, M. Ding, S. Philippe, Y. Ning, *ChemRxiv.* **2020**, DOI 10.26434/chemrxiv.13414691.v1.
[24] A. Giannikos, P. Petrolekas, C. Pliangos, A. Frenzel, C. G. Vayenas, H. Pütter, *Ionics* **1998**, *4*, 161–169.
[25] a) G. Kyriakou, M. B. Boucher, A. D. Jewell, E. A. Lewis, T. J. Lawton, A. E. Baber, H. L. Tierney, M. Flytzani-Stephanopoulos, E. C. H. Sykes, *Science* **2012**, *335*, 1209–1212; b) M. D. Marcinkowski, A. D. Jewell, M. Stamatakis, M. B. Boucher, E. A. Lewis, C. J. Murphy, G. Kyriakou, E. C. H. Sykes, *Nat. Mater.* **2013**, *12*, 523–528.
[26] M. Xiong, Z. Gao, P. Zhao, G. Wang, W. Yan, S. Xing, P. Wang, J. Ma, Z. Jiang, X. Liu, J. Ma, J. Xu, Y. Qin, *Nat. Commun.* **2020**, *11*, 4773.
[27] a) K.-D. Jung, A. T. Bell, *J. Catal.* **2000**, *193*, 207–223; b) C. Mao, J. Wang, Y. Zou, G. Qi, J. Y. Yang Loh, T. Zhang, M. Xia, J. Xu, F. Deng, M. Ghoussoub, N. P. Kherani, L. Wang, H. Shang, M. Li, J. Li, X. Liu, Z. Ai, G. A. Ozin, J. Zhao, L.

Zhang, *J. Am. Chem. Soc.* **2020**, *142*, 17403–17412; c) C. Wang, E. Guan, L. Wang, X. Chu, Z. Wu, J. Zhang, Z. Yang, Y. Jiang, L. Zhang, X. Meng, B. C. Gates, F.-S. Xiao, *J. Am. Chem. Soc.* **2019**, *141*, 8482–8488; d) N. Rui, F. Zhang, K. Sun, Z. Liu, W. Xu, E. Stavitski, S. D. Senanayake, J. A. Rodriguez, C.-J. Liu, *ACS Catal.* **2020**, *10*, 11307–11317.

[28] a) F. Chen, X. Jiang, L. Zhang, R. Lang, B. Qiao, *Chin. J. Catal.* **2018**, *39*, 893–898; b) W. C. Conner, J. L. Falconer, *Chem. Rev.* **1995**, *95*, 759–788; c) H. Zhang, X. Chang, J. G. Chen, W. A. Goddard, B. Xu, M.-J. Cheng, Q. Lu, *Nat. Commun.* **2019**, *10*, 3340; d) J. Gao, H. Zhang, X. Guo, J. Luo, S. M. Zakeeruddin, D. Ren, M. Grätzel, *J. Am. Chem. Soc.* **2019**, *141*, 18704–18714; e) L. DeRita, J. Resasco, S. Dai, A. Boubnov, H. V. Thang, A. S. Hoffman, I. Ro, G. W. Graham, S. R. Bare, G. Pacchioni, X. Pan, P. Christopher, *Nat. Mater.* **2019**, *18*, 746–751; f) L. DeRita, S. Dai, K. Lopez-Zepeda, N. Pham, G. W. Graham, X. Pan, P. Christopher, *J. Am. Chem. Soc.* **2017**, *139*, 14150–14165; g) X. Zhang, M. Zhang, Y. Deng, M. Xu, L. Artiglia, W. Wen, R. Gao, B. Chen, S. Yao, X. Zhang, M. Peng, J. Yan, A. Li, Z. Jiang, X. Gao, S. Cao, C. Yang, A. J. Kropf, J. Shi, J. Xie, M. Bi, J. A. van Bokhoven, Y.-W. Li, X. Wen, M. Flytzani-Stephanopoulos, C. Shi, W. Zhou, D. Ma, *Nature* **2021**, *589*, 396–401.

Manuscript received: June 4, 2022
Accepted manuscript online: July 17, 2022
Version of record online: ■■, ■■

Forschungsartikel

Heterogeneous Catalysis

M. J. Hülsey, V. Fung, X. Hou, J. Wu, N. Yan* **e202208237**

Hydrogen Spillover and Its Relation to Hydrogenation: Observations on Structurally Defined Single-Atom Sites

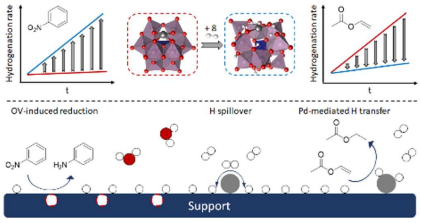

In contrast to common belief, hydrogen spillover can be either beneficial or detrimental to the catalytic performance of hydrogenation catalysts. This was determined through in-depth studies of structurally well-defined single-atom catalysts as well as conventional Pt/WO_3.